




ORIGINAL ARTICLE OPEN ACCESS

Genomic and Transcriptomic Characterization of Protein Kinase C Fusion Melanocytic Neoplasms With Distinctive Hypopigmented Histomorphology: A Single-Institution Study

Aofei Li¹  | Brandon Umphress¹ | Carina Dehner¹ | Ryan Jones²  | Keller Toral² | Simon Warren^{1,3} | Ahmed K. Alomari^{1,3} 

¹Department of Pathology and Laboratory Medicine, Indiana University School of Medicine, Indianapolis, Indiana, USA | ²Tempus Labs Inc., Chicago, Illinois, USA | ³Department of Dermatology, Indiana University School of Medicine, Indianapolis, Indiana, USA

Correspondence: Ahmed K. Alomari (akalomar@iu.edu)

Received: 19 September 2024 | **Revised:** 16 February 2025 | **Accepted:** 17 February 2025

Keywords: melanocytic neoplasm | molecular pathology | Protein Kinase C

ABSTRACT

Background: Genomic fusions involving Protein Kinase C (*PKC* or *PRKC*) have been classically identified in a subset of melanocytic neoplasms with heavy melanin pigmentation as described in older series. They were recently reclassified from the pigmented epithelioid melanocytoma (PEM) category to the blue nevus (BN) category in the fifth edition of the World Health Organization (WHO) Classification of Skin Tumors.

Methods: Herein, we report a series of eight mostly hypopigmented *PRKC* fusion melanocytic tumors with novel comprehensive molecular characterization. Clinical, histopathologic, and immunohistochemical findings were reviewed. Next-generation sequencing (NGS) data on genomic and transcriptomic levels were explored.

Results: Histomorphology showed a biphasic pattern with hypercellular areas and hypocellular areas with dense fibrotic stroma and collagen trapping. The clinical courses were uncomplicated after excisions. NGS revealed three cases of *PRKCB* fusion and five cases of *PRKCA* fusions. RNA differential analysis against six blue nevi showed a group of genes with significantly higher transcription levels and strong enrichment in the direct p53 effectors gene set. *PRKC* fusion tumors also demonstrated significantly stronger p53 IHC staining.

Conclusion: We further expand the morphologic spectrum of *PRKC* fusion melanocytic tumors and provide insight into their morphologic identification. Our novel transcriptome-level findings provide insight into the nuanced molecular events and new evidence for classification.

1 | Introduction

With the advent of accessible genomic profiling of challenging melanocytic neoplasms, important and clinically relevant genotypic–phenotypic correlations are being described. A better

understanding of these entities is critical for accurate diagnosis, management, and long-term prognostication. Moreover, the recent World Health Organization (WHO) classifications of melanocytic tumors emphasize the importance of driver mutation identification for proper classification [1].

Aofei Li and Brandon Umphress contributed equally to this study.

This is an open access article under the terms of the [Creative Commons Attribution-NonCommercial-NoDerivs](https://creativecommons.org/licenses/by-nc-nd/4.0/) License, which permits use and distribution in any medium, provided the original work is properly cited, the use is non-commercial and no modifications or adaptations are made.

© 2025 The Author(s). *Journal of Cutaneous Pathology* published by John Wiley & Sons Ltd.

PRKC fusions as a driver of melanocytic neoplasia have only been recently described, particularly in the context of genomic analysis of pigmented epithelioid melanocytomas (PEM) [2, 3]. PEM is characterized histopathologically by pigmented epithelioid melanocytes with vesicular nuclei and marked associated melanophages [4, 5]. At the molecular level, *PRKC* fusions were suggested as one of two main pathways underpinning the development of PEMs, with the other one being the inactivating mutation of *PRKARIA*. In these reports, tumors with *PRKC* fusion were morphologically distinct as they showed a sheet-like growth pattern with a predominance of pigmented melanocytes over melanophages and an absent conventional nevus component. They are recently reclassified from the *PRKARIA*-associated PEM category to the *GNAQ/GNA11*-driven blue nevus (BN) category in the fifth edition of the WHO Classification of Skin Tumors, based on the belief that PKC acts downstream of *GNAQ* [6]. In part, this reflects the evolving understanding of these tumors and their characteristics.

In a 2023 study, the histopathologic and genetic features of 51 melanocytic neoplasms with *PRKC* fusion genes were characterized [7]. Forty-two tumors were classified as benign, three tumors (including two proliferating nodules) were considered intermediate grade, and six tumors were classified as melanomas with sheets of atypical melanocytes infiltrating the dermis (notably, two of the melanomas demonstrated BAP1 loss by immunohistochemistry). The benign lesions were characterized by a biphasic dermal proliferation with nests of small melanocytes, surrounding fibrosis, and associated spindled dendritic melanocytes (resembling combined blue nevi). Notably, 60% of the tumors were heavily pigmented and 15% of cases had hyperpigmented epithelioid melanocytes at the dermo-epidermal junction, while a minority of cases were described as with subtle pigment.

The use of molecular investigative tools has enabled more in-depth characterization of *PRKC* fusion tumors. In a 2024 study, principal component analysis on transcriptomic data showed higher similarity between five *PRKC* fusion tumors and four blue nevi as opposed to two PEMs with *PRKARIA* mutations [8]. While the findings were interesting, further RNA differential analysis results were not reported. Statistically significant differential analysis of *PRKC* fusion tumors and blue nevi likely has been precluded by the small sample size in that study.

Herein, we report eight cases of *PRKC* fusion tumors with mostly hypopigmented biphasic morphology and novel, distinct transcriptome-level features corroborated by protein-level evidence with strong statistical significance. We believe that this study is an important addition to the evolving knowledge of tumors driven by *PRKC* fusions.

1 | Methods

1.1 | Selection of Cases

As part of routine clinical workup, challenging or unusual melanocytic neoplasms were evaluated by genomic and transcriptomic analysis if deemed necessary by consensus dermatopathology examination to help in further classification and

management recommendations. From 2017 to 2024, cases with *PRKC* fusion were identified and were further reviewed by four board-certified dermatopathologists. This study has been approved by our institutional review board.

For comparative studies (immunohistochemistry and transcriptome analysis described below), a group of six conventional blue nevi with *GNAQ/GNA11* mutations was selected from the same cohort described above in a consecutive case fashion based on material (tissue block and sequencing data) availability.

1.2 | Clinical Data

Demographic data (age, gender), clinical information (primary lesion size, location, appearance), and follow-up data, including lesion-specific treatment, were reviewed in the institutional electronic medical record database.

1.3 | Immunohistochemistry

Immunohistochemical staining was performed on 4- μ m formalin-fixed, paraffin-embedded sections using the following antibodies: p16, HMB45, Melan-A, Melan-A/Ki-67, and BAP-1. Immunohistochemical testing was performed on an Agilent Omnis instrument using immunoperoxidase-based immunohistochemistry for the following antibodies: SOX10 (clone EP268; Dako), HMB-45 (clone HMB-45; Dako), p16 (clone JC2; Cell Marque), PRAME (clone EPR20330; Abcam), Ki67/Melan-A dual stain (clone MIB-1 and clone A103; Dako), BAP1(C-4 clone, Santa Cruz) and p53 (DO-7 clone, Dako).

1.4 | Comparative p53 Immunohistochemistry Analysis

Comparative p53 immunohistochemistry was performed on the *PRKC* fusion tumor group and the *GNAQ/GNA11* tumor group. All tumors were also part of the transcriptome analysis described below. The results were interpreted in a simplified H-score fashion: staining intensity of the nuclei (0: negative, 1+: weak, 3+: strong) and the corresponding tumor cells percentage (0%–100%) were evaluated by two reviewing pathologists blinded to the diagnosis independently. Staining scores were calculated by multiplying the intensity with the percentage of positive cells, yielding scores ranging from 0 to 300. Averaged staining scores from the two reviewers were compared between the two groups using student's *t*-test. A *p*-value of less than 0.05 was considered significant. The representative images were digitally enhanced with photoshop 2023 (Adobe Inc.) to suppress the blue chromogen signal and enhance the red chromogen signal in a uniform fashion for better publication quality while retaining data fidelity. This process did not influence quantitative scoring as it took place afterward.

1.5 | DNA And RNA Sequencing

Cases deemed appropriate for molecular testing for diagnostic purposes as described above were sent to Tempus Labs Inc. for

DNA and RNA sequencing using the Tempus xT and xR assays (Tempus Labs Inc.), as previously described [9–11].

1.6 | Transcriptome Analysis

To study the transcriptomic-level difference between the *PRKC* fusion tumors and the *GNAQ/GNA11* tumors, RNA data from both tumor groups were derived from the same Tempus xR assay platform protocol. Quantile normalization was performed for optimal comparability. Targets with total counts of less than 50 reads across all samples were filtered out to ensure data quality. Whole transcriptome differential expression analysis was performed with the limma-voom method [12]. Statistical and bioinformatical analysis was performed using R (v4.3.0) and BiocManager (release 3.17). The Benjamini-Hochberg (BH) procedure was used to adjust for false discovery in multiple comparisons. Gene set enrichment analysis was performed with GeneAnalytics. Enrichment results with an adjusted *p*-value smaller than 0.0001 were considered significant [13].

2. | Results

2.1 | Clinical and Histopathological Results

The clinical and histopathological features of these tumors are summarized in Table 1. Representative cases are illustrated in Figures 1–4. The cohort consisted of six females and two males ranging in age from 1 to 54 years with a wide anatomic distribution. These tumors ranged in size from 0.3 to 6.0 cm. Remarkably, Case 8 presented with a 6.0-cm congenital dark brown plaque with a 2.5-cm thickened central area (Figure 4G). Tumors were dermal based with no to minimal lentiginous junctional component. Most cases showed an elevated plaque-like silhouette with irregular deep borders. Three had bulbous tongue-like projections into the deep dermis or subcutis, similar to that seen in cellular blue nevi. All tumors were characterized by a distinctive biphasic growth pattern present in variable amounts and distributions. The biphasic pattern consisted of hypercellular and hypocellular areas. The hypercellular area showed sheeted aggregates of melanocytes with minimal intervening stroma and largely nevic/small epithelioid cytomorphology, some with band-like distribution. The hypocellular area was characterized by a loose proliferation of oval-to-spindled melanocytes within a fibrotic stroma with features of “collagen trapping” toward the periphery of the lesion (Figures 2C and 4D). In both areas, there was minimal cytologic atypia and mitoses were rare (Figures 1–3). In all cases except Case 8, the melanocytes in these tumors had minimal or light melanin pigmentation, and associated melanophages were sparse, whereas in Case 8, prominent melanin pigment was present both in melanocytes and in melanophages (Figure 4E,F). In one case (Case 6), we observed prominent desmin-positive smooth muscle hyperplasia significantly exceeding the expected amount of background arrector pili, admixed with the tumor cells in a similar fashion that has been reported recently (Figure 4A–C) [14]. Five patients underwent excision of their tumors with negative margins, while two opted for observation based on clear biopsy margins. One patient was planned to undergo excision. After an

average of 23 months of follow-up, no patient showed evidence of local recurrence, regional, or distant metastases.

2.2 | Immunohistochemistry

Immunohistochemistry was performed to further evaluate each case (Table 1). p16 demonstrated retained expression in all cases, with one case showing diminished expression (Case 4, Figure 3E). Melan-A/Ki-67 performed on seven cases demonstrated a very low proliferative index. Additionally, HMB45 performed on six cases had a diffuse staining pattern with no stratification. BAP1 was retained in all cases. Importantly, the sheeted and hypocellular areas demonstrated identical staining characteristics.

2.3 | Genomic-Level Findings

Next-generation sequencing identified three cases of *PTPRJ::PRKCB* fusion and five cases of *PRKCA* fusions with partners *SLC44A1*, *RNF13*, *ATP2B4*, and *SCARB1*. The fusion partners scattered across the genome involve Chromosomes 1, 3, 9, 11, and 12. These fusion partners are recurrent as have been reported in the literature [7, 8]. Additional pathogenic genetic alterations were rare and sporadic, including an *ATM* stop-gain mutation. The available cases showed a low mutation burden (0.5–3.7/MB, average 1.9/MB, 2nd–50th percentile).

2.4 | Transcriptomic-Level Findings

With proper normalization, quality control, and false discovery adjustment, RNA differential expression analysis of the eight *PRKC* fusion tumors against six *GNAQ/GNA11*-driven blue nevi showed a group of genes with significantly higher transcription levels (adjusted *p* < 0.05), including *CCNG1*, *BAX*, *CDK6*, and *GDF15* (Figure 5). Gene set pathway analysis of this group of genes showed significant enrichment in direct p53 effectors (SuperPath database, adjusted *p* < 0.0001). This group of genes also showed strong enrichment to adenocarcinoma gene sets, including prostate adenocarcinoma, breast adenocarcinoma, and lung adenocarcinoma (adjusted *p* < 0.0001).

Meanwhile, the *PRKC* fusion tumors showed another group of genes with significantly lower transcription levels compared to blue nevi (adjusted *p* < 0.05), including *KIF1A*, *MICAL1*, *TUBB2A*, and *TRPC6* (Figure 5). This group of genes showed significant enrichment in “response to elevated cytosolic calcium” in gene set pathway analysis (adjusted *p* < 0.0001).

2.5 | Functional Protein-Level Findings

Encouraged by the unexpected findings of p53 pathway differences between *PRKC* fusion tumors and blue nevi at the transcriptomic level, we further pursued assessment of such differences at the protein level using p53 immunohistochemistry. Comparative quantitative p53 immunohistochemistry was performed in the two groups. Nuclear staining scores in *PRKC* fusion tumors (median score = 24.8) were significantly higher

TABLE 1 | Summary of clinical, pathological, and molecular findings of PRKC fusion melanocytic neoplasms.

| Case | Age | Gender | Clinical | | Biphasic | | | Deep border | Pigmentation | IHC findings | Fusion | Additional pathogenic alterations | TMB (percentile) |
|------|-----|--------|----------------------|--|---|-------------------|----------------------|---------------------------------------|-----------------|---|-----------------------|-----------------------------------|------------------|
| | | | Location | lesion | Follow-up | pattern of growth | Silhouette | | | | | | |
| 1 | 17 | M | Post-auricular scalp | 1.2-cm lesion, traumatized | Re-excision with negative margins; NED at 86 months of follow-up | Present | Elevated plaque like | Irregular with bulbous projections | Minimal pigment | p16 retained, Melan-A/Ki-67 low proliferation, HMB-45 without gradient of maturation. BAP1 retained | <i>PTPRJ::PRKCB</i> | N/A | N/A |
| 2 | 7 | F | Right upper eyelid | 0.3-cm elevated lesion present for 4 years | Margins free on biopsy; clinical follow-up to-date with no known recurrence at 18 months | Present | Exophytic/polypoid | Flat | Light pigment | p16 retained, Melan-A/Ki-67 low proliferation, HMB45 without stratification, BAP-1 retained | <i>ATP2B4::PRKCA</i> | None | 2.1/MB (18th) |
| 3 | 32 | F | Right chest wall | 0.6-cm raised dark papule | Margins free on biopsy; on Pembrolizumab for Stage II breast invasive ductal carcinoma Clinical follow-up to-date with no known recurrence at 18 months | Present | Elevated plaque like | Irregular with no bulbous projections | Light pigment | p16 retained, Melan-A/Ki-67 low proliferation, HMB45 without stratification, PRAME negative, BAP-1 retained | <i>PTPRJ::PRKCB</i> | <i>ATM</i> p.R1730 stop gain | 1.6/MB (12th) |
| 4 | 50 | F | Left ankle | 0.8-cm skin colored papule | Re-excision with negative margins; NED at 22 months follow-up | Present | Elevated plaque like | Cannot be assessed | Minimal pigment | p16 diminished, HMB-45 without stratification, BAP-1 retained | <i>SLC44A1::PRKCA</i> | None | 3.7/MB (50th) |
| 5 | 54 | F | Right shoulder | 0.4-cm gray brown thin papule | Re-excision with negative margins; NED at 8 months follow-up | Present | Elevated plaque like | Irregular with no bulbous projections | Light pigment | p16 retained, Melan-A/Ki-67 low proliferation, HMB-45 without stratification. BAP-1 retained PRAME scattered positive | <i>RNF13::PRKCA</i> | None | 2.1/MB (18th) |

(Continues)

TABLE 1 | (Continued)

| Case | Age | Gender | Location | Clinical lesion | Biphasic pattern of growth | | | Deep border | Pigmentation | IHC findings | Fusion | Additional pathogenic alterations | TMB (percentile) |
|------|-----|--------|--------------------------|--|--|------------|----------------------|---------------------------------------|---------------|--|--------------|-----------------------------------|------------------|
| | | | | | Follow-up | Silhouette | | | | | | | |
| 6 | 38 | F | Right posterior shoulder | 0.8-cm deep brown to black papule | Re-excision with negative margins; NED at 7 months follow-up | Present | Elevated plaque like | Irregular with no bulbous projections | Light pigment | BAP-1 retained | RNF13::PRKCA | None | 1.6/MB (11th) |
| 7 | 49 | F | Right groin | 0.5-cm dark brown papule | Re-excision with negative margins; NED at 2 months follow-up | Present | Elevated plaque like | Irregular with bulbous projections | Light pigment | p16 retained, Melan-A/Ki-67 low proliferation, HMB-45 without stratification. BAP-1 retained | PTPRJ::PRKCB | N/A | N/A |
| 8 | 1 | M | Scalp | Congenital 6.0-cm dark brown plaque with 2.5-cm central nodularity | Planned for re-excision, no evidence of tumor regrowth in 2 months | Present | Elevated plaque like | Irregular with bulbous projections | Heavy pigment | p16 retained, Melan-A/Ki67 slightly increased index at 3%, PRKAR1A and BAP1 retained, PRAME negative | SCAR1::PRKCA | None | 0.5/MB (2nd) |

than in blue nevi (median score = 3.2) ($p < 0.0023$, Student's t -test) (Figure 6).

3 | Discussion

PRKC is involved in the signal transduction of receptor-mediated hydrolysis of phospholipids to regulate various cellular homeostatic mechanisms, including apoptosis, migration, and proliferation [15–17]. Fusions involving *PRKC* are not unique to melanocytic neoplasia, as there are previously described non-melanocytic tumors with such fusions [18]. Examples include papillary glioneuronal tumor, benign fibrous histiocytoma, lung squamous cell carcinoma, lung adenocarcinoma, and low-grade glioma, among others [18–21].

In melanocytic neoplasia, these fusions are usually associated with heavily pigmented melanocytic neoplasms. In older literature, they were included in the category of PEM. In this context, they were usually “pure” PEMs with no associated precursor nevus [3]. Furthermore, PEM with *PRKCA* fusion has been reported to occur more commonly in younger patients with histopathologic features of monomorphic epithelioid-shaped melanocytes with moderate-grade nuclear atypia and higher mitotic activity [2]. In the upcoming WHO Classification of Skin Tumors, melanocytic neoplasms driven by *PRKCA* fusions are classified along the BN lineage unless an associated *PRKAR1A* mutation is present [6]. This is based on recent studies and anecdotal data showing better clustering of their gene expression profiles with blue nevi [8].

We identified eight cases of melanocytic neoplasms with a consistent biphasic histopathologic pattern. These tumors demonstrate a dermal-based proliferation of medium-sized epithelioid/oval cells with distinct areas of increased cellularity and a sheet-like pattern of growth alternating with areas with less compact oval/spindled melanocytes and fibrotic stroma. In contrast to older literature, our cases mostly demonstrated minimal to light pigmentation, except for only one case with heavy pigmentation. Individual melanocytes mostly demonstrate small nucleoli and indistinct cell membranes. Mitotic activity was low, and significant cytologic atypia was lacking. Toward the periphery of these lesions, areas of prominent collagen trapping were frequently identified. In all of these cases, a *PRKC* fusion was identified. Compared to the previously reported data on *PRKC* fusions in melanocytic neoplasia, our cases strikingly differ in terms of their degree of pigmentation, rarity of atypia, and alternating areas of hypercellularity and hypocellularity. Some of these differences are likely related to our methodology of selecting these cases from a cohort of primary (rather than consultative) melanocytic neoplasms with unusual but not necessarily worrisome features.

Despite extensive research in the literature, the exact role of *PRKC* in oncogenesis has been controversial, with the most recent evidence supporting it as a tumor suppressor, given most *PRKC* point mutations are loss-of-function [22, 23]. For *PRKC* fusion, however, this appears rather counter-intuitive given the features of genomic-level findings both in our series and the literature. The pathogenic *PRKC* fusion constructs have been found to be recurrent, in-frame, with intact functional domains,

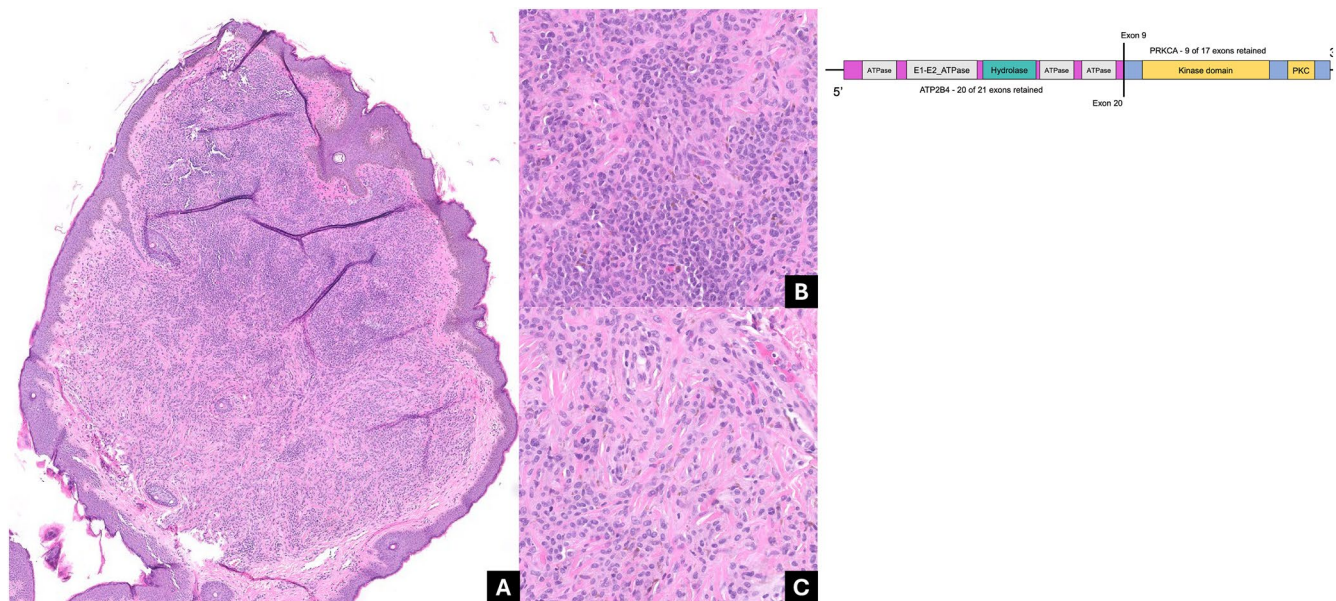


FIGURE 1 | Representative histomorphology of *PRKC* fusion tumors (Case 2). (A) Low power view shows dermal melanocytic proliferation with biphasic hypercellular and hypocellular areas (20×, H&E). (B) High power view shows hypercellular areas with epithelioid cells and light melanin pigment (200×, H&E). (C) High power view shows hypocellular areas with spindle cells and collagen trapping (200×, H&E). (D) Schematic showing *ATP2B4::PRKCA* in-frame fusion with retained kinase domain.

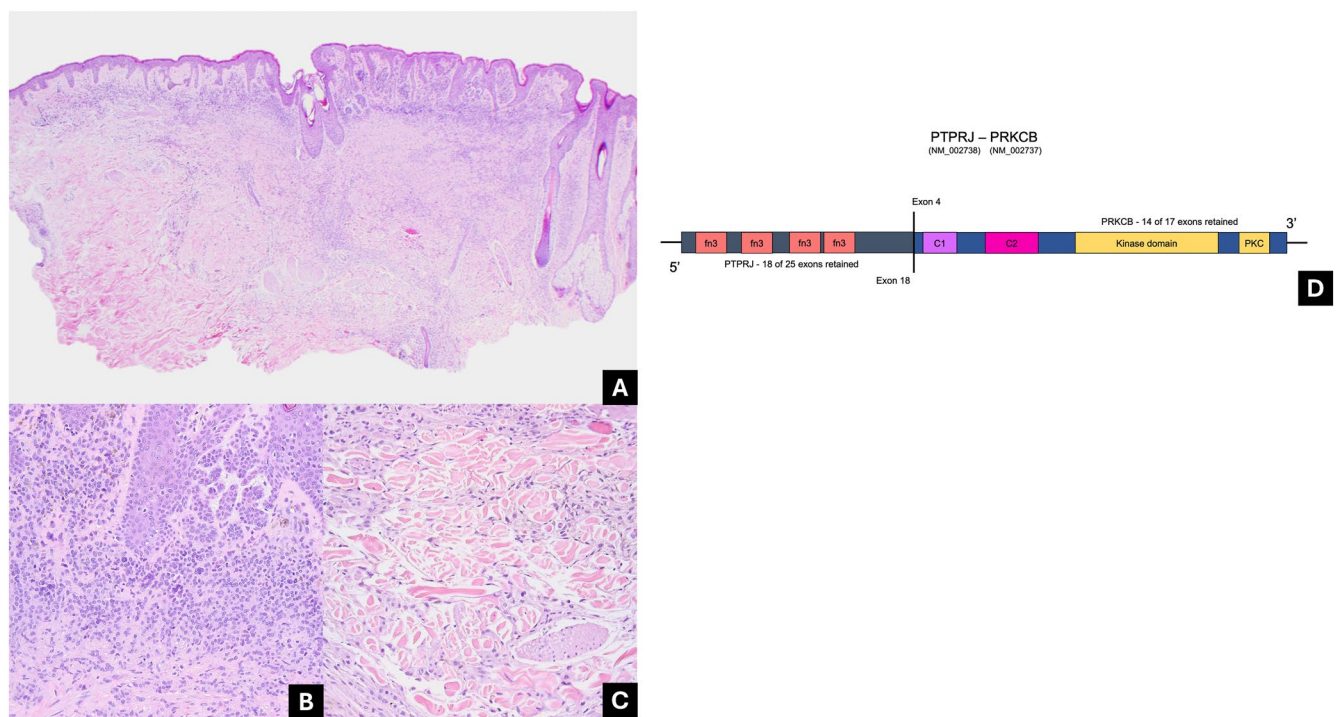


FIGURE 2 | Representative histomorphology of *PRKC* fusion tumors (Case 3). (A) Low power view shows dermal melanocytic proliferation with a band-like distribution, as well as biphasic hypercellular and hypocellular areas (20×, H&E). (B) High power view shows hypercellular areas with epithelioid cells and light melanin pigment (200×, H&E). (C) High power view shows hypocellular areas with spindle cells and collagen trapping (200x H&E). (D) Schematic showing *PTPRJ::PRKCB* in-frame fusion with retained kinase domain.

indicating that retained function, rather than loss-of-function, is required for oncogenesis, a trait frequently seen in oncogenes but not in tumor suppressors. However, this might be explained by a potential dominant negative effect of the fusion protein. Interestingly, recent data have demonstrated that *PRKC* fusions

may be distinct from other oncogenic fusions as their presence may result in overall loss of function [22]. This hypothesis is further supported by the finding that CRISPR/Cas9-mediated fusion *PRKC* protein demonstrates marked instability [24]. Our differential RNA analysis revealed significant relative

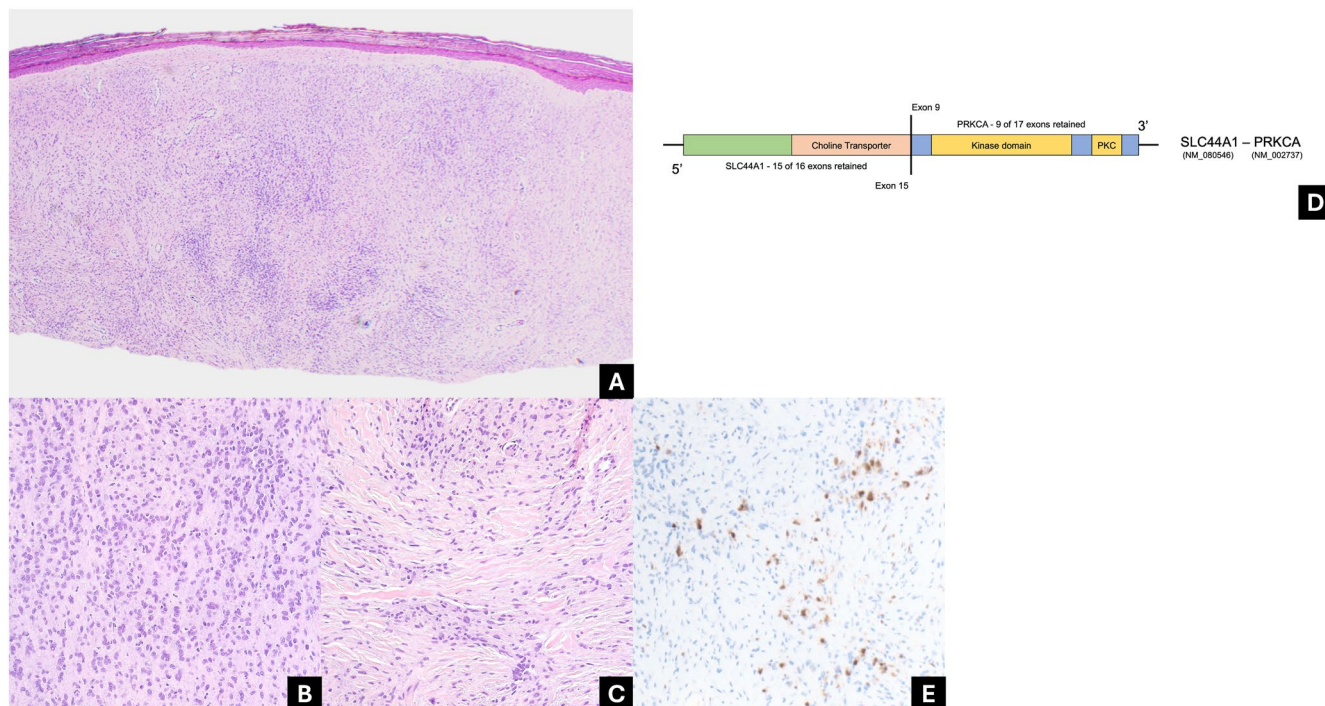


FIGURE 3 | Representative histomorphology of *PRKC* fusion tumors (Case 4). (A) Low power view shows dermal melanocytic proliferation with biphasic hypercellular and hypocellular areas (20×, H&E). (B) High power view shows hypercellular areas with epithelioid cells and minimal melanin pigment (200×, H&E). (C) High power view shows hypocellular areas with spindle cells (200×, H&E). (D) Schematic showing *SLC44A1::PRKCA* in-frame fusion with retained kinase domain. (E) High power view shows diminished patchy p16 immunohistochemistry.

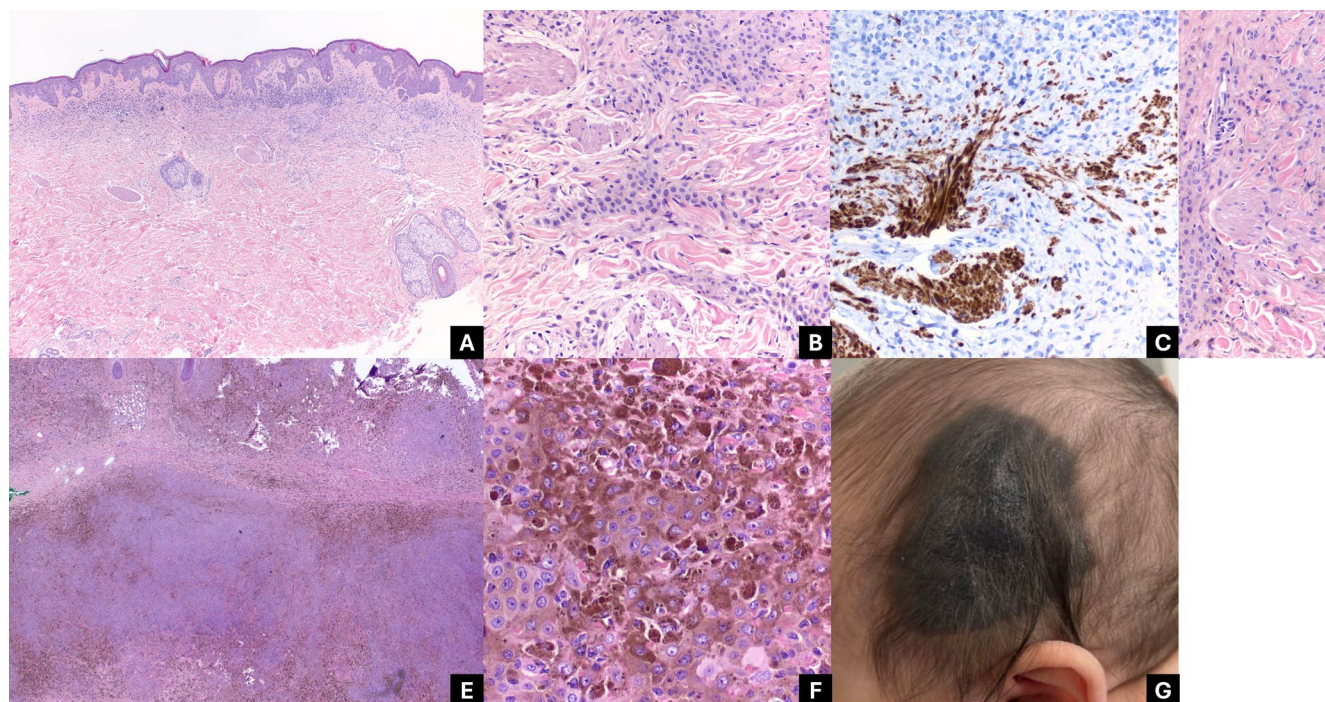


FIGURE 4 | Unusual histomorphology and clinical findings of *PRKC* fusion tumors (Cases 6 and 8). (A) Case 6: low power view shows dermal melanocytic proliferation with a band-like distribution, as well as biphasic hypercellular and hypocellular areas (20×, H&E). (B) Case 6: high power view shows prominent smooth muscle hyperplasia and biphasic melanocytic architectural pattern, light melanin pigment (200×, H&E). (C) Case 6: desmin immunostain highlights smooth muscle hyperplasia. (D) Case 6: high power view shows hypocellular area with collagen trapping pattern. (E) Case 8: low power view shows dermal nodular melanocytic proliferation with biphasic hypercellular and hypocellular areas (20×, H&E). (F) Case 8: high power view shows heavy melanin pigment in both melanocytes and melanophages (400×, H&E). (G) Clinical findings of Case 8: 6-cm dark brown plaque on left scalp with central nodularity.

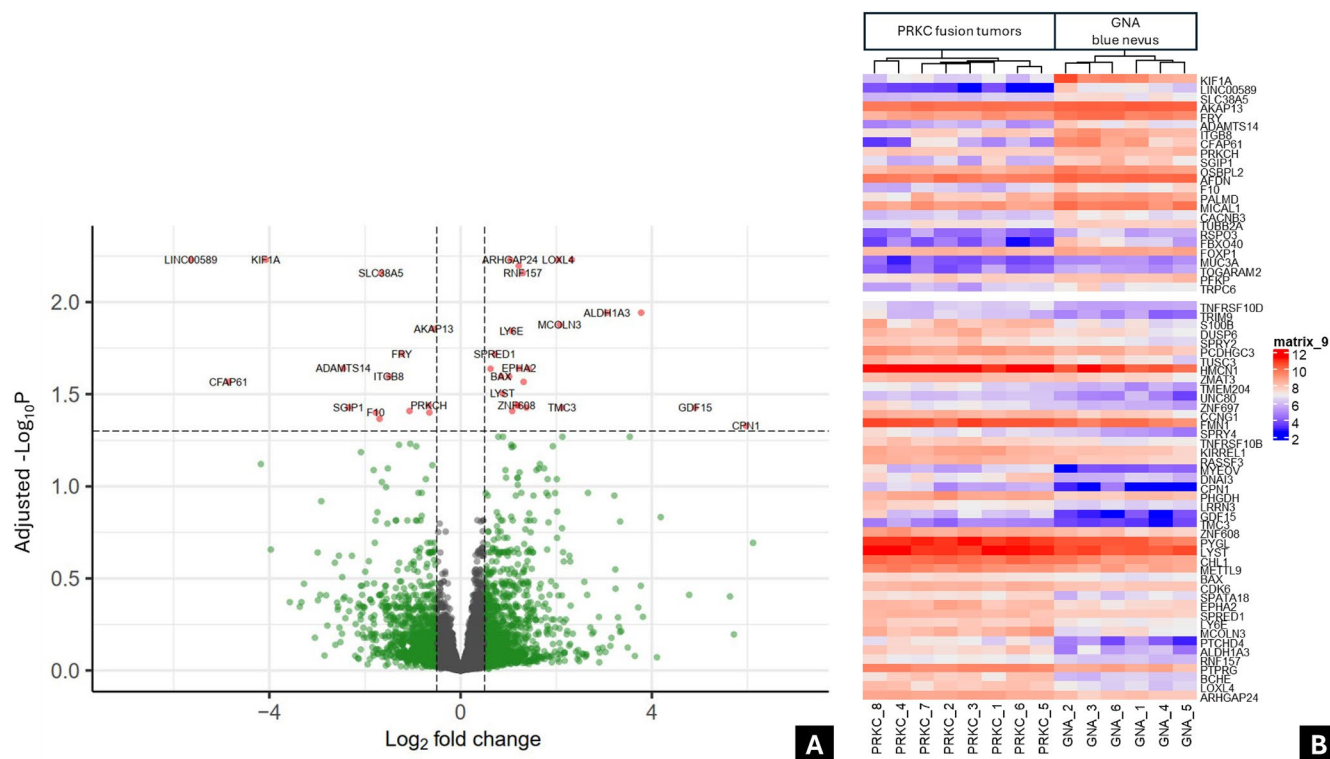


FIGURE 5 | Transcriptomic comparison of *PRKC* fusion tumors against blue nevi. (A) Volcano plot showing numerous statistically significant differentially expressed genes after false discovery adjustment (vertical axis indicates raw *p*-value on a Log10 scale; horizontal axis indicates transcript fold change on a Log2 scale), (B) Heatmap showing top significant differentially expressed genes (adjusted *p*-value < 0.05).

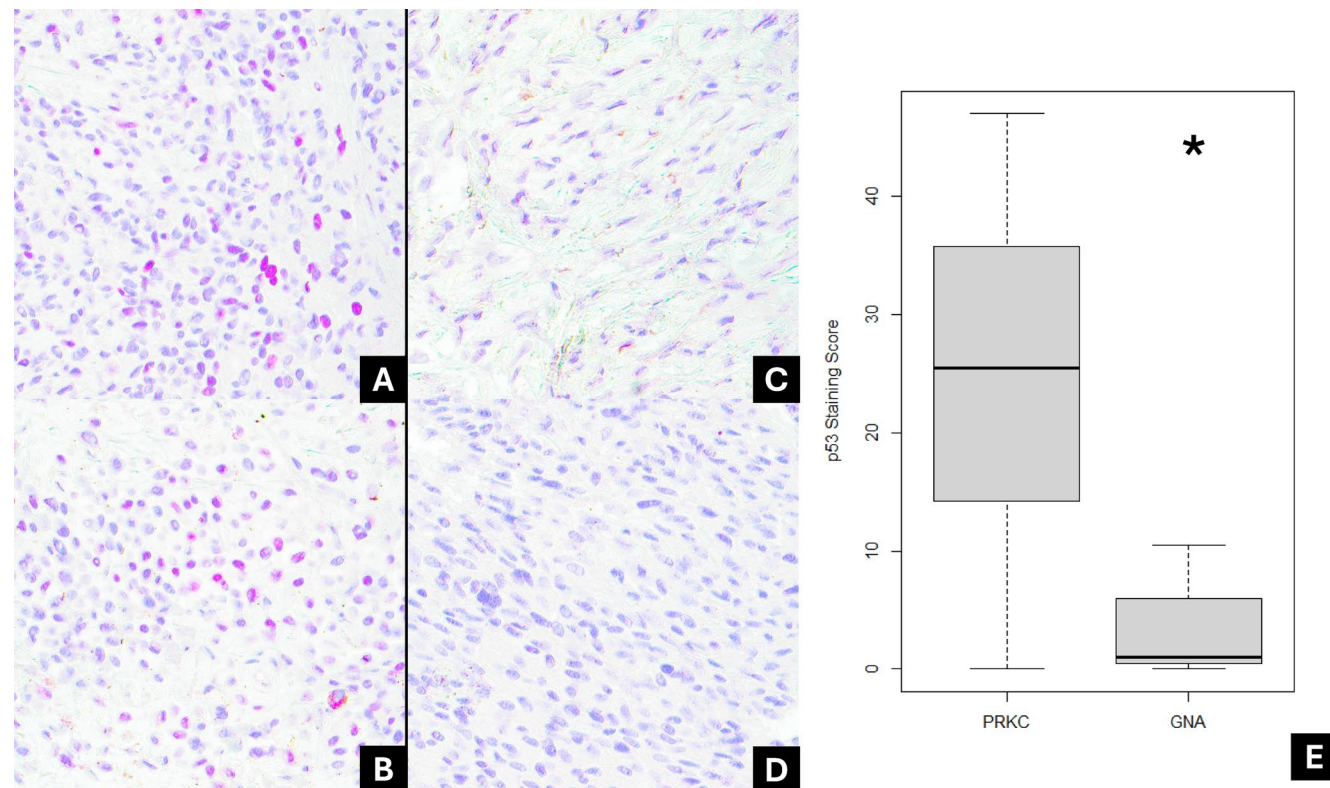


FIGURE 6 | Comparative p53 IHC of *PRKC* fusion tumors against blue nevi. (A, B) Representative *PRKC* fusion tumors (Cases 3 and 4) show patchy nuclear p53 staining. (C, D) Representative blue nevi show diffusely negative p53 staining (uniformly enhanced digitally). (E) Boxplot showing eight *PRKC* fusion tumors (left) with significantly higher p53 staining scores compared against six blue nevi (right) (mean 24.8 vs. 3.2, **p* < 0.0023).

downregulation of “response to elevated cytosolic calcium” gene set in *PRKC* fusion tumors compared to blue nevi. Interestingly, *PRKC* activation plays a major role in “response to elevated cytosolic calcium.” [25] This transcriptomic-level finding suggests that *PRKC* fusion may also disrupt physiological *PRKC* pathway participants. In line with the current understanding in the literature, our findings may in part support that physiological *PRKC* activation has tumor suppressive effects that are paradoxically antagonized by pathologic *PRKC* fusion protein actions. Further studies are required to explore this conjecture. Although GNAQ is believed to play a role in *PRKC* upstream activation, the exact pathogenic role of *PRKC* appears more intricate than merely an oncogenic element on a tandem pathway.

Apart from *PRKC* pathway differences, our transcriptomic-level study also revealed significantly stronger p53 pathway activation in *PRKC* fusion tumors compared to blue nevi. This finding is corroborated by a significantly stronger p53 immunohistochemistry staining in *PRKC* fusion tumors compared to blue nevi. This protein-level experiment also complements our RNA analysis through higher quantitative resolution, where individual cells were analyzed for the nuclear p53 protein staining, excluding noises introduced by impurities in bulk sequencing. The demonstration of stronger nuclear p53 protein staining, combined with no p53-related abnormalities on the genomic level, also indicates that the p53 pathway activation in *PRKC* fusion tumors is likely incited by events upstream of p53 protein expression. In other words, *PRKC* fusion likely triggers certain molecular events that result in a reactive p53 protein overexpression that in turn activates the downstream intact p53 pathway. This cascade of molecular events is relatively lacking in blue nevi compared to *PRKC* fusion tumors. *PRKC*-p53 crosstalk has been studied in the past few decades, with most literature suggesting that certain isoforms of *PRKC* can activate p53 through protein phosphorylation [26–28]. It has also been reported that *PRKC* can upregulate p53 gene transcription [29]. The latter is in accordance with our findings, although p53 protein phosphorylation, which was not evaluable with our methods, may possibly also play a role in *PRKC* fusion tumors. Interestingly, the activation of the p53 pathway renders *PRKC* fusion tumor transcriptomic semblance to prostate adenocarcinoma, breast adenocarcinoma, and lung adenocarcinoma, which was detected in our RNA gene set enrichment study. Despite this, we believe p53 immunohistochemistry has limited utility in the clinical diagnosis of *PRKC* fusion tumors as the staining is weak and patchy (has a median score of 24.8 out of a maximum of 300). Although this degree of staining has statistical significance for scientific evidence in this cohort, such difference may not be reliable enough for routine diagnostic use in individual cases. Moreover, we have not explored the intensity and pattern of p53 staining in other potential histopathological mimickers.

Previously, melanomas had been rarely associated with *PRKC* fusions; however, six cases were recently described, two of which demonstrated BAP-1 loss. As the reporting institutions of these six melanoma cases likely have a bias toward more atypical consultation-based neoplasms, it might still be true that identifying a *PRKCA* or *PRKCB* fusion would suggest a low risk for progression to melanoma [18, 30]. Nevertheless, since malignant transformation is possible and well documented in the

literature, careful examination for worrisome histopathologic features is important. Complete excision of these tumors is generally recommended.

Limitations in this study include the following. Our sample size is medium, potentially limiting the statistical power in some studies. Bulk RNA sequencing is subject to non-tumor cell contaminations, although the lack of prominent lymphocytic infiltrate mitigates such contaminations. Although statistically significant, the p53 nuclear staining intensity was generally not strong, limiting our image quality to some extent.

In summary, we expand the spectrum of tumors driven by *PRKC* fusions to include neoplasms with minimal to light pigmentation. We believe these results will contribute to improved understanding and ongoing characterization of these tumors. Ultimately, this will enable informed communication between dermatopathologists and treating physicians regarding the diagnosis, management, and prognostication of such tumors. Our findings on both the RNA and protein levels demonstrate the nuanced molecular events in *PRKC* fusion tumors that are distinct from blue nevi and therefore provide new evidence for classification.

Author Contributions

Ahmed K. Alomari conceptualized and designed the project, collected the data, reviewed parts of clinical information, and revised the manuscript. Aofei Li supplemented the project design, performed the bioinformatic analysis, reviewed parts of clinical information, complied parts of the data, and wrote parts of the manuscript. Brandon Umphress provided diagnostic support, reviewed parts of clinical information, complied parts of the data, and wrote parts of the manuscript. Carina Dehner collected the data, provided diagnostic support, and reviewed the manuscript. Simon Warren collected the data, provided diagnostic support, and reviewed the manuscript. Ryan Jones and Keller Toral provided fusion gene schematics. All authors approved the final manuscript.

Acknowledgments

We thank Jamunabai Maruvathu Prakash from IU Health Pathology Laboratory for conducting p53 immunohistochemistry.

Ethics Statement

This study has been approved by our Institutional Review Board.

Conflicts of Interest

Brandon Umphress is a consultant pathologist for Tempus Labs, however, unrelated to this work. No other conflicts to disclose.

Data Availability Statement

The data that support the findings of this study are available from the corresponding author upon reasonable request.

References

1. D. E. Elder, B. C. Bastian, I. A. Cree, D. Massi, and R. A. Scolyer, “The 2018 World Health Organization Classification of Cutaneous, Mucosal, and Uveal Melanoma: Detailed Analysis of 9 Distinct Subtypes Defined by Their Evolutionary Pathway,” *Archives of Pathology & Laboratory*

- Medicine 144, no. 4 (2020): 500–522, <https://doi.org/10.5858/arpa.2019-0561-RA>.
2. M. C. Isales, L. S. Mohan, V. L. Quan, et al., “Distinct Genomic Patterns in Pigmented Epithelioid Melanocytoma: A Molecular and Histologic Analysis of 16 Cases,” *American Journal of Surgical Pathology* 43, no. 4 (2019): 480–488, <https://doi.org/10.1097/PAS.0000000000001195>.
3. J. N. Cohen, N. M. Joseph, J. P. North, C. Onodera, A. Zembowicz, and P. E. LeBoit, “Genomic Analysis of Pigmented Epithelioid Melanocytomas Reveals Recurrent Alterations in PRKAR1A, and PRKCA Genes,” *American Journal of Surgical Pathology* 41, no. 10 (2017): 1333–1346, <https://doi.org/10.1097/PAS.0000000000000902>.
4. A. Zembowicz, J. A. Carney, and M. C. Mihm, “Pigmented Epithelioid Melanocytoma: A Low-Grade Melanocytic Tumor With Metastatic Potential Indistinguishable From Animal-Type Melanoma and Epithelioid Blue Nevus,” *American Journal of Surgical Pathology* 28, no. 1 (2004): 31–40, <https://doi.org/10.1097/00000478-200401000-00002>.
5. A. Zembowicz, S. M. Knoepf, T. Bei, et al., “Loss of Expression of Protein Kinase a Regulatory Subunit 1alpha in Pigmented Epithelioid Melanocytoma But Not in Melanoma or Other Melanocytic Lesions,” *American Journal of Surgical Pathology* 31, no. 11 (2007): 1764–1775, <https://doi.org/10.1097/PAS.0b013e318057faa7>.
6. WHO Classification of Tumours Editorial Board, “Skin Tumours,” in *WHO Classification of Tumours Series*, vol. 12, 5th ed. (International Agency for Research on Cancer, 2023).
7. A. Fouchardiere, D. Pissaloux, A. Houlier, et al., “Histologic and Genetic Features of 51 Melanocytic Neoplasms With Protein Kinase C Fusion Genes,” *Modern Pathology* 36, no. 11 (2023): 100286, <https://doi.org/10.1016/j.modpat.2023.100286>.
8. P. Patel, A. Chen, N. Sharma, et al., “PRKC Fusion Melanocytic Tumors, a Subgroup of Melanocytic Tumors More Closely Aligned to Blue Nevus Than to PRKAR1A-Inactivated Pigmented Epithelioid Melanocytomas,” *American Journal of Surgical Pathology* 48, no. 11 (2024): 1349–1358, <https://doi.org/10.1097/PAS.0000000000002262>.
9. N. Beaubier, R. Tell, R. Huether, et al., “Clinical Validation of the Tempus xO Assay,” *Oncotarget* 9, no. 40 (2018): 25826–25832.
10. N. Beaubier, R. Tell, D. Lau, et al., “Clinical Validation of the Tempus xT Next-Generation Targeted Oncology Sequencing Assay,” *Oncotarget* 10, no. 24 (2019): 2384–2396.
11. A. K. Alomari, P. W. Harms, A. A. Andea, and S. J. Warren, “MAP2K1-Mutated Melanocytic Tumors Have Reproducible Histopathologic Features and Share Similarities With Melanocytic Tumors With BRAF V600E Mutations,” *Journal of Cutaneous Pathology* 50, no. 12 (2023): 1083–1093, <https://doi.org/10.1111/cup.14502>.
12. C. W. Law, Y. Chen, W. Shi, and G. K. Smyth, “Voom: Precision Weights Unlock Linear Model Analysis Tools for RNA-Seq Read Counts,” *Genome Biology* 15, no. 2 (2014): R29, <https://doi.org/10.1186/gb-2014-15-2-r29>.
13. S. Ben-Ari Fuchs, I. Lieder, G. Stelzer, et al., “GeneAnalytics: An Integrative Gene Set Analysis Tool for Next Generation Sequencing, RNAseq and Microarray Data,” *OMICS: A Journal of Integrative Biology* 20, no. 3 (2016): 139–151.
14. D. Goutas, P. Hayenne, F. Tirode, D. Pissaloux, I. Yeh, and A. de la Fouchardiere, “Smooth Muscle Hyperplasia in Protein Kinase C-Fused Blue Naevi: Report of 12 Cases,” *Histopathology* 85 (2024): 347–352.
15. E. C. Dempsey, A. C. Newton, D. Mochly-Rosen, et al., “Protein Kinase C Isozymes and the Regulation of Diverse Cell Responses,” *American Journal of Physiology. Lung Cellular and Molecular Physiology* 279, no. 3 (2000): L429–L438, <https://doi.org/10.1152/ajplung.2000.279.3.L429>.
16. R. Garg, L. G. Benedetti, M. B. Abera, H. Wang, M. Abba, and M. G. Kazanietz, “Protein Kinase C and Cancer: What We Know and What We Do Not,” *Oncogene* 33, no. 45 (2014): 5225–5237, <https://doi.org/10.1038/onc.2013.524>.
17. E. M. Griner and M. G. Kazanietz, “Protein Kinase C and Other Diacylglycerol Effectors in Cancer,” *Nature Reviews. Cancer* 7, no. 4 (2007): 281–294, <https://doi.org/10.1038/nrc2110>.
18. N. Stransky, E. Cerami, S. Schalm, J. L. Kim, and C. Lengauer, “The Landscape of Kinase Fusions in Cancer,” *Nature Communications* 5 (2014): 4846, <https://doi.org/10.1038/ncomms5846>.
19. J. A. Bridge, X. Q. Liu, J. Sumegi, et al., “Identification of a Novel, Recurrent SLC44A1-PRKCA Fusion in Papillary Glioneuronal Tumor,” *Brain Pathology* 23, no. 2 (2013): 121–128, <https://doi.org/10.1111/j.1750-3639.2012.00612.x>.
20. A. Plaszczyca, J. Nilsson, L. Magnusson, et al., “Fusions Involving Protein Kinase C and Membrane-Associated Proteins in Benign Fibrous Histiocytoma,” *International Journal of Biochemistry & Cell Biology* 53 (2014): 475–481, <https://doi.org/10.1016/j.biocel.2014.03.027>.
21. J. Luo, D. Gu, H. Lu, S. Liu, and J. Kong, “Coexistence of a Novel PRKCB-ALK, EML4-ALK Double-Fusion in a Lung Adenocarcinoma Patient and Response to Crizotinib,” *Journal of Thoracic Oncology: Official Publication of the International Association for the Study of Lung Cancer* 14, no. 12 (2019): e266–e268, <https://doi.org/10.1016/j.jtho.2019.07.021>.
22. A.-A. N. Van, M. T. Kunkel, T. R. Baffi, et al., “Protein Kinase C Fusion Proteins Are Paradoxically Loss of Function in Cancer,” *Journal of Biological Chemistry* 296 (2021): 1–18.
23. P. J. Parker, S. J. Brown, V. Calleja, et al., “Equivocal, Explicit and Emergent Actions of PKC Isoforms in Cancer,” *Nature Reviews Cancer* 21, no. 1 (2021): 51–63.
24. A.-A. N. Van, M. T. Kunkel, T. R. Baffi, C. E. Antal, and A. C. Newton, “Protein Kinase C Fusions Reveal Another Mechanism for Loss of Protein Kinase C Function in Cancer,” *FASEB Journal* 34, no. S1 (2020): 1.
25. Y. Takai, A. Kishimoto, Y. Iwasa, Y. Kawahara, T. Mori, and Y. Nishizuka, “Calcium-Dependent Activation of a Multifunctional Protein Kinase by Membrane Phospholipids,” *Journal of Biological Chemistry* 254, no. 10 (1979): 3692–3695.
26. I. Coutinho, G. Pereira, M. Leão, J. Gonçalves, M. Côrte-Real, and L. Saraiva, “Differential Regulation of p53 Function by Protein Kinase C Isoforms Revealed by a Yeast Cell System,” *FEBS Letters* 583, no. 22 (2009): 3582–3588.
27. K. Yoshida, H. Liu, and Y. Miki, “Protein Kinase C δ Regulates Ser46 Phosphorylation of p53 Tumor Suppressor in the Apoptotic Response to DNA Damage,” *Journal of Biological Chemistry* 281, no. 9 (2006): 5734–5740.
28. J. Baudier, C. Delphin, D. Grunwald, S. Khochbin, and J. J. Lawrence, “Characterization of the Tumor Suppressor Protein p53 as a Protein Kinase C Substrate and a S100b-Binding Protein,” *Proceedings of the National Academy of Sciences of the United States of America* 89, no. 23 (1992): 11627–11631.
29. H. Liu, Z.-G. Lu, Y. Miki, and K. Yoshida, “Protein Kinase C δ Induces Transcription of the TP53 Tumor Suppressor Gene by Controlling Death-Promoting Factor Btf in the Apoptotic Response to DNA Damage,” *Molecular and Cellular Biology* 27, no. 24 (2007): 8480–8491.
30. J. Zhao, N. Lampley, 3rd, S. Benton, et al., “Next-Generation Sequencing Reveals a New Class of Melanocytic Neoplasms With Hybrid Genomic Features of PEM Including Protein Kinase R1 Alpha Gene Inactivation and Spitz Tumor-Defining Protein Kinase Fusions,” *American Journal of Dermatopathology* 44, no. 8 (2022): 568–574, <https://doi.org/10.1097/DAD.0000000000002223>.